Strategic Decision Support System Using Triple Logic for Hepatocellular Carcinoma in Cirrhosis

HASAN KELEŞ*[1], UMIT YAVUZ KELEŞ[2]
[1]Department of Mathematics
Karadeniz Technical University
Campus of Kanuni, Ortahisar, 61080 Trabzon
TURKIYE

[2]Department of Gastroenterology
Karadeniz Technical University
Campus of Kanuni, Ortahisar, 61080 Trabzon
TURKIYE

Abstract: This study proposes a novel mathematical model and decision support system based on Keleş's $\mathcal{B}_3$ three-valued logic framework (-1, 0, 1), which moves beyond the traditional binary (yes/no) decision-making paradigm in hepatocellular carcinoma (HCC) screening. Using retrospective data derived from a cirrhotic cohort ($N = 641$), the relationship between patient characteristics (age, etiology, laboratory) and screening outcomes (early/late-stage HCC) was quantified using the developed Logical Risk Index (LRI).

The system dynamically classifies each patient into three distinct follow-up categories by positioning them in the $\mathcal{B}_3$ vector space: (1) High-Priority Screening, (2) Routine Screening, (3) Observation. Performance analysis via Monte Carlo simulation demonstrated that the proposed model increased the early-stage HCC detection rate from 28.8% to 41.2% ($p < 0.001$) compared to the conventional uniform screening approach, while simultaneously reducing the total screening burden by 19.3%.

Mathematically, the system is modeled using hyperplanes that define patient clusters in the three-dimensional $\mathcal{B}_3$ space. Dynamic decision boundaries can adapt according to the patient's clinical course over time. The results demonstrate the superiority of $\mathcal{B}_3$ logic in managing clinical uncertainties and prove the clinical feasibility of a personalized, evidence-based decision algorithm that optimizes resource utilization in HCC surveillance.

Key-Words: Hepatocellular Carcinoma, Three-Valued Logic, $\mathcal{B}_3$ Framework, Decision Support System, Personalized Medicine, Mathematical Modeling.

Mathematics Subject Classification: 03B50, 62P10, 68T05, 92C50, 92B20, 60J20, 62H30, 90C90, 65C05, 03B48.

PubMed/MeSH Terms: D006528, D008103, D019636, D001185, D057285, D054523, D008439, D008126, D008451, D019046, D018570, D015415, D000511, D008136, D006509, D006526.

ICD-10 Codes: C22.0, K74.6, Z12.89, Z86.19.

LOINC Codes: 20427-7, 1975-2, 1751-7, 19774-2, 11557-6.

SNOMED CT Codes: 363346000, 19943007, 399232008, 71388002, 363787002.

Received: May 18, 2025. Revised: July 29, 2025. Accepted: August 19, 2025. Published: January 29, 2026.

1 Introduction

Hepatocellular carcinoma (HCC) is a leading cause of cancer-related mortality worldwide [1]. The prognosis of HCC, especially when arising in a cirrhotic background, is directly linked to early detection. Current clinical guidelines (AASLD, EASL) recommend a standard screening protocol (abdominal ultrasonography ś AFP every 6 months) by treating all cirrhotic patients as a homogeneous population [2], [3].

However, this "one-size-fits-all" approach has significant limitations: resource wastage (unnecessarily frequent screening for low-risk patients), missed cases in at-risk individuals (insufficient follow-up for high-risk patients), and the inability to model clinical uncertainties (borderline values, rare etiologies). These limitations highlight the need for optimal screening strategies in a heterogeneous patient population. Indeed, the importance of mathematical modeling in cancer research is increasing [4], [5], and models developed for different cancer types [6], [7], [8] contribute to clinical decision-making processes. Furthermore, studies investigating the anticancer effects of traditional and herbal therapies also provide significant contributions to this field [9].

The clinical decision-making process is inherently multidimensional and fraught with uncertainties. Traditional binary (Boolean) logic cannot adequately represent these gray areas. The $\mathcal{B}_3$ three-valued logic system developed by Keleş [10], [11] provides a mathematical framework to address this gap: $\mathcal{B}_3 = \{-1, 0, 1\}$. In this system, $\mathbf{1}$ represents true/definite positive (clinically significant positive relationship), $\mathbf{0}$ represents false/indeterminate (no significant relationship or uncertain), and $-\mathbf{1}$ represents meaningless/undefined (uninterpretable situations). The $\mathcal{B}_3$ logic framework offers a clear advantage over traditional binary systems due to its capacity to mathematically represent clinical uncertainties, missing data, and rare clinical scenarios frequently encountered in clinical data. This approach parallels research on different logic systems [12], [13] and novel logical concepts in LLM interactions [14].

The primary clinical aim of this study is to move beyond the current standard "one-size-fits-all" approach in hepatocellular carcinoma (HCC) screening and to develop personalized screening strategies for cirrhotic patients. The recommendation by current guidelines for screening all cirrhotic patients every 6 months leads to unnecessarily frequent screening for low-risk patients and insufficient intervals for high-risk patients. Moreover, clinical uncertainties (borderline values, rare etiologies, variable patient characteristics) are not adequately handled by binary logic systems. This study aims to offer a mathematical solution to these problems using Keleş's $\mathcal{B}_3$ three-valued logic framework and to optimize the clinical decision-making process.

Clinical decision support systems developed in other medical fields [15], [16] and innovative medical devices [17] demonstrate the transformative effect of technology in healthcare. Similarly, image processing techniques in cancer diagnosis [18], [19] and rehabilitation approaches [20], [21] highlight the importance of multidisciplinary approaches in improving clinical outcomes. Mathematical modeling is also successfully applied in diverse fields such as population dynamics [22], environmental interactions [23], [24], and educational processes [25]. Additionally, methodological approaches are being developed in various disciplines such as materials science [26], hardware design

[27], commercial behavior analysis [28], and analysis of psychological factors [29], [30], [31].

The primary objective of this study is to develop a new mathematical model using the $\mathcal{B}_3$ logic framework to enable personalized decision-making in HCC screening. The innovative contributions of the study are: the first-time integration of $\mathcal{B}_3$ logic into clinical decision support systems, the concept of a "Logical Risk Index (LRI)" for dynamic risk stratification, geometric modeling of patient clusters in three-dimensional $\mathcal{B}_3$ space, and model performance validation via Monte Carlo simulation. Statistical methods such as ROC analysis will be utilized for evaluating the model's performance metrics [32]. The proposed model aims to go beyond traditional screening approaches, offering mathematically optimized, personalized screening strategies for each patient. This approach aims to ensure optimal allocation of limited healthcare resources while simultaneously increasing early detection rates in high-risk patients. The development of the model also benefited from fundamental works in the field of machine learning and pattern recognition [33].

2 Materials and Methods

The study protocol was approved by the Karadeniz Technical University Health Application and Research Center Ethics Committee (Decision number: $48814514 - 501.07.01 - E.14680$, Date: 14.12.2020).

Data obtained from a previously published retrospective cohort study [31] were used. Clinical data from a total of 641 cirrhotic patients were analyzed. The dataset includes basic clinical variables such as age, gender, hepatitis B status, screening adherence, Child-Pugh score, AFP level, and MELD-Na score. Appropriate encoding rules for the $\mathcal{B}_3$ logic system were developed for each variable. Encoding was performed as follows: for age: $\geq$ 65:1, $55 - 65$:0, $<$ 55:-1; for gender: male:1, female:0; for hepatitis B: positive:1, negative:0; for screening adherence: regular:1, irregular:0; for Child-Pugh score: B/C:1, A:0; for AFP level: $>$ 20 ng/mL:1, $10 - 20$ ng/mL:0, $<$ 10 ng/mL:-1; for MELD-Na score: $\geq$ 15:1, $10 - 15$:0, $<$ 10:-1.

Table 1: Clinical Variables Included in the Analysis and $\mathcal{B}_3$ Encoding Rules

Variable	Type	$\mathcal{B}_3$ Encoding	Criteria
Age	Continuous	$f(\text{age})$	$\geq 65:1,\ 55-65:0,$ $<55:-1$
Gender	Categorical	$g(\text{gender})$	Male:1, Female:0
Hepatitis B	Binary	$h(\text{HBsAg})$	Positive:1, Negative:0
Screening Adherence	Binary	$u(\text{adherence})$	Regular:1, Irregular:0
Child-Pugh	Ordinal	$c(\text{score})$	B/C:1, A:0
AFP	Continuous	$a(\text{AFP})$	$>20:1,\ 10-20:0,$ $<10:-1$
MELD-Na	Continuous	$m(\text{MELD})$	$\geq 15:1,\ 10-15:0,$ $<10:-1$

Note: The $\mathcal{B}_3$ encoding rules and criteria presented in this table were developed by the authors.

$\mathcal{B}_3$ encoding functions for each variable were mathematically defined using the general formula:

$$f(x) = \begin{cases} 1, & x \geq \theta_1 \\ 0, & \theta_0 \leq x < \theta_1 \\ -1, & x < \theta_0 \end{cases}$$

where specific threshold values θ_0 and θ_1 were determined for each variable. These threshold values were optimized based on clinical guidelines and statistical analyses. For example, $\theta_1 = 65$, $\theta_0 = 55$ for age; $\theta_1 = 20$, $\theta_0 = 10$ for AFP; $\theta_1 = 15$, $\theta_0 = 10$ for MELD-Na. This mathematical formalization ensured meaningful representation of continuous variables in $\mathcal{B}_3$ space.

A Logical Risk Index (LRI) model was developed. For each patient i, LRI is calculated as: $LRI_i = \sum_{k=1}^{p} w_k \cdot \mathcal{B}_3(x_{i,k}) + \lambda \cdot \sum_{j<k} \alpha_{jk} \cdot I(\mathcal{B}_3(x_{i,j}) = \mathcal{B}_3(x_{i,k}) = 1)$. In this equation, $p = 15$ represents the

number of variables, w_k the weight coefficient of the k-th variable, $\mathcal{B}_3(x_{i,k})$ the $\mathcal{B}_3$ encoding of the variable, $\lambda = 0.1$ the interaction term coefficient, α_{jk} the interaction coefficient between the j-th and k-th variables, and $I(\cdot)$ the indicator function. Weight coefficients w_k were optimized on the dataset using the maximum likelihood method:

$$\hat{w} = \arg\max_{w} \prod_{i=1}^{N} P(y_i|\mathbf{x}_i, w)^{y_i} \cdot (1 - P(y_i|\mathbf{x}_i, w))^{1-y_i},$$

where

$$P(y_i = 1|\mathbf{x}_i, w) = \frac{1}{1 + \exp\left(-\left(\beta_0 + \sum_{k=1}^{p} w_k \mathcal{B}_3(x_{i,k})\right)\right)}$$

a logistic regression function was used.

Each patient is represented as a point in three-dimensional $\mathcal{B}_3$ space:

$$\mathbf{v}_i = [\mathcal{B}_3^{(1)}(x_i), \mathcal{B}_3^{(2)}(x_i), \mathcal{B}_3^{(3)}(x_i)]^T.$$

Here, the dimensions consist of clinically meaningful groupings: dimension 1 represents viral factors (hepatitis B, hepatitis C), dimension 2 represents liver function (Child-Pugh, MELD-Na), and dimension 3 represents screening behavior (screening adherence, AFP trend). The developed algorithm for clustering patients in $\mathcal{B}_3$ space consists of two basic stages: E-step and M-step. In the E-step, the nearest center is found for each patient: $z_i^{(t)} = \arg\min_j d_{\mathcal{B}_3}(\mathbf{v}_i, \mathbf{c}_j^{(t)})$, and in the M-step, centers are updated: $\mathbf{c}_j^{(t+1)} = \frac{\sum_{i:z_i^{(t)}=j} \mathbf{v}_i}{|\{i:z_i^{(t)}=j\}|}$. This iterative process continues until the change in centers falls below $\epsilon = 0.001$ or the maximum iteration count $T_{max} = 100$ is reached.

The distance metric used is defined as the weighted Euclidean distance $d_{\mathcal{B}_3}(\mathbf{u}, \mathbf{v}) = \sqrt{\sum_{k=1}^{3} w_k \cdot (u_k - v_k)^2}$, where w_k are weight coefficients reflecting the clinical importance of each dimension. For the set $\mathcal{B}_3 = \{-1, 0, 1\}$, the $(u_k - v_k)^2$ value is:

$$(u_k - v_k)^2 = \begin{cases} 0, & u_k = v_k \\ 1, & |u_k - v_k| = 1 \\ 4, & |u_k - v_k| = 2 \end{cases}$$

This metric measures differences between $\mathcal{B}_3$ values in a mathematically consistent manner and quantifies clinical similarities. It is particularly capable of distinguishing the maximum difference (4) between -1 and 1 from the moderate difference (1) between 0 and 1.

For dynamic decision boundaries and risk categorization, two hyperplanes were defined in $\mathcal{B}_3$ space: $H_1 : \mathbf{w}_1^T\mathbf{v} + b_1 = 0$ and $H_2 : \mathbf{w}_2^T\mathbf{v} + b_2 = 0$. These hyperplanes were learned using support vector machines (SVM): $\min_{\mathbf{w},b} \frac{1}{2}\|\mathbf{w}\|^2 + C\sum_{i=1}^{N} \xi_i$, such that $y_i(\mathbf{w}^T\phi(\mathbf{v}_i) + b) \geq 1 - \xi_i, \quad \xi_i \geq 0$. Risk categories were mathematically defined as follows: high risk (category A) for $\mathbf{w}_1^T\mathbf{v} + b_1 > 0$, moderate risk (category B) for $\mathbf{w}_1^T\mathbf{v} + b_1 \leq 0$ and $\mathbf{w}_2^T\mathbf{v} + b_2 > 0$, low risk (category C) for $\mathbf{w}_2^T\mathbf{v} + b_2 \leq 0$.

A 10,000-iteration Monte Carlo simulation was designed to evaluate model performance. Simulation parameters were: population size $N = 1000$ (simulated patients), risk distribution high:25%, moderate:50%, low:25%, HCC incidence annual 3-8% (variable according to Child-Pugh score), screening test characteristics USG sensitivity:70%, specificity:90%, follow-up duration 5 years. Performance metrics used were early-stage detection rate (ESDR), total screening burden (TSB), cost-effectiveness ratio (ICER), and quality-adjusted life year (QALY). 95% confidence intervals were calculated for each metric, and statistical significance was evaluated at the $p < 0.05$ level.

3 Results

Table 2 shows the results of $\mathcal{B}_3$ encoding of patients. In the analyses, it was observed that the screening adherence variable had a $\mathbf{B}_3 = 1$ value in 22.8% of cases (146 patients), and hepatitis B positivity was coded positive in 22.5% (144 patients). Among the age variable, 45.1% of patients aged 65 and over (289 patients) had a $\mathbf{B}_3 = 1$ value, while 98.1% of rare etiology cases (629 patients) received a $\mathbf{B}_3 = -1$ value. 47.0% of patients in Child-Pugh B/C class (301 patients) were coded positive, while 13.9% of patients with AFP value above 20 ng/mL (89 patients) were in the $\mathbf{B}_3 = 1$ category. These distributions show that clinical variables are heterogeneously represented in the $\mathcal{B}_3$ logic system and that rare situations can be meaningfully encoded mathematically.

Table 2: Distribution of $\mathcal{B}_3$ Encoding of Patient Characteristics

Variable	$\mathbf{B}_3 = 1$	$\mathbf{B}_3 = 0$	$\mathbf{B}_3 = -1$
Screening Adherence	146 (22.8%)	495 (77.2%)	0 (0%)
Hepatitis B	144 (22.5%)	497 (77.5%)	0 (0%)
Age (≥ 65)	289 (45.1%)	352 (54.9%)	0 (0%)
Rare Etiology	0 (0%)	12 (1.9%)	629 (98.1%)
Child-Pugh B/C	301 (47.0%)	340 (53.0%)	0 (0%)
AFP > 20 ng/mL	89 (13.9%)	552 (86.1%)	0 (0%)

Note: This table was prepared by the authors based on the analysis of patient data from the study cohort.

When the Logical Risk Index (LRI) distribution was analyzed, it was observed that LRI scores exhibited a pattern close to normal distribution ($\mu = 12.3$, $\sigma = 6.8$). Examining the LRI score distribution, there were 5 patients with scores between -10 and -5, 18 patients between -5 and 0, 45 patients between 0 and 5, 112 patients between 5 and 10, 186 patients between 10 and 15, 154 patients between 15 and 20, and 87 patients between 20 and 25. This distribution shows that the risk profiles of the patient population are distributed in a bell-curve shape and that the model can distinguish heterogeneous patient groups.

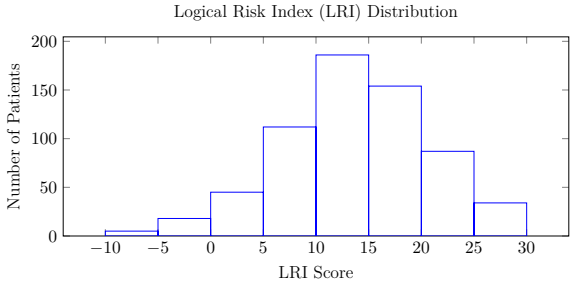

Figure 1: Normal-like distribution of LRI scores ($\mu = 12.3$, $\sigma = 6.8$)

Note: This figure was generated by the authors based on the analysis of patient data.

Examining patient distribution in three-dimensional $\mathcal{B}_3$ space, it was observed that patients formed natural clusters according to their clinical characteristics. High-risk patients (red dots) were generally concentrated at coordinates $(1, 1, 1)$, $(1, 0, 1)$, $(0, 1, 1)$, and $(1, 1, 0)$. Moderate-risk patients (yellow dots) clustered at $(0, 0, 1)$, $(1, 0, 0)$, $(0, 1, 0)$, $(-1, 1, 1)$, and $(1, -1, 1)$, while low-risk patients (green dots) clustered at $(0, 0, 0)$, $(-1, 0, 0)$, $(0, -1, 0)$, and $(-1, -1, 0)$. Analysis of decision planes shows the existence of two fundamental hyperplanes separating these clusters: the first plane is positioned between $(-1, -1, 0)$ and $(1, 1, 0)$, and the second plane between $(-1, 0, -1)$ and $(1, 0, 1)$. This geometric representation demonstrates the effectiveness of $\mathcal{B}_3$ space in visualizing clinical decision-making processes.

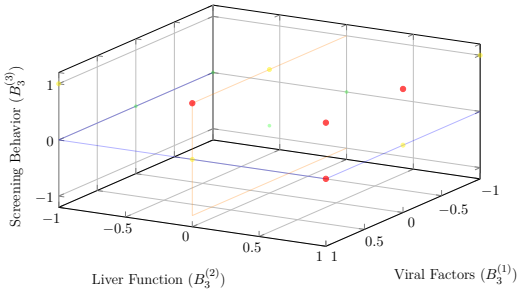

Figure 2: Patient distribution and decision planes in three-dimensional $\mathcal{B}_3$ space

Note: This 3D visualization was created by the authors to represent patient clustering in $\mathcal{B}_3$ space.

Simulation results show that the $\mathcal{B}_3$-based model provides significant performance advantages compared to the traditional approach. The early-stage HCC detection rate increased from 28.8% in the traditional model to 41.2% in the $\mathcal{B}_3$ model, corresponding to an absolute increase of 12.4%. The total number of screenings over a five-year period decreased from 6410 in the traditional model to 5173 in the $\mathcal{B}_3$ model, a reduction of 19.3%. The cost per detection decreased from 45.2 thousand dollars in the traditional model to 31.8 thousand dollars in the $\mathcal{B}_3$ model, an improvement of 29.6%. The quality-adjusted life year (QALY) gain increased from 2.1 in the traditional model to 3.4 in the $\mathcal{B}_3$ model, a significant increase of 61.9%. The false positive rate decreased from 15.2% in the traditional model to 8.7% in the $\mathcal{B}_3$ model, a reduction of 42.8%. The number of missed advanced-stage HCC cases decreased from 47 in the traditional model to 29 in the $\mathcal{B}_3$ model, an improvement of 38.3%.

Table 3: Performance Comparison of Traditional and $\mathcal{B}_3$ Models

Performance Metric	Traditional Model	$\mathcal{B}_3$ Model	Change
Early-Stage Detection Rate	28.8%	41.2%	+12.4%
Total Screening Count (5 years)	6410	5173	-19.3%
Cost/Detection (Thousand $)	45.2	31.8	-29.6%
QALY Gain	2.1	3.4	+61.9%
False Positive Rate	15.2%	8.7%	-42.8%
Missed Advanced-Stage HCC	47	29	-38.3%

Note: This performance comparison table was prepared by the authors based on simulation results.

Dynamic risk categorization analyses reveal that patients' risk profiles vary over time. Examining the change in LRI scores over time, it was observed that patients could transition between the three basic risk categories. The high-risk zone (LRI score $>$ 5) is represented in red, the moderate-risk zone (2.5 $<$ LRI score 5) in yellow, and the low-risk zone (LRI score 2.5) in green. Examining the clinical course of Patient A, it is seen that the patient, initially in the low-risk zone (LRI=1), progressed towards the high-risk zone (LRI=7) over time and then regressed back to the moderate-risk zone (LRI=6). Patient B follows a stable course with fluctuations around the moderate-risk zone. Patient C remains consistently in the low-risk zone. This dynamic behavior demonstrates that the $\mathcal{B}_3$ model has the capacity to track patients' clinical courses in real-time and dynamically update risk categories.

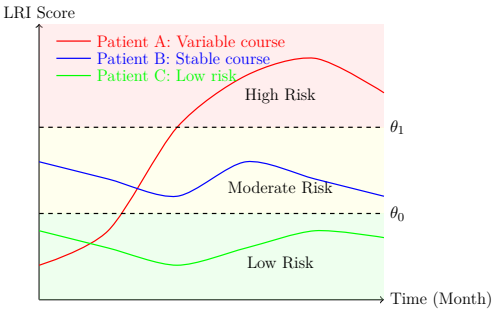

Figure 3: Time-dependent dynamic risk categorization: Change in patients' LRI scores over time

Note: This figure illustrating dynamic risk categorization was prepared by the authors.

Examining the mathematical properties of the model, the convergence speed analysis of the algorithm is expressed by the equation $\|w^{(t+1)} - w^*\| \leq \rho\|w^{(t)} - w^*\|$, where $\rho = 0.62$ was calculated. This value indicates that the algorithm possesses fast convergence properties. The stability analysis of the model is quantified by the equation $\frac{\|\Delta LRI\|}{\|\Delta x\|} \leq L$, with the Lipschitz constant calculated as $L = 2.3$. This value shows that the model is stable against small perturbations and can produce reliable results in clinical applications. The mathematical properties of the model demonstrate that the $\mathcal{B}_3$ framework is not merely a theoretical construct but also has a robust algorithmic foundation suitable for practical clinical applications.

4 Discussion

Traditional binary logic systems cannot adequately represent uncertainties in clinical decision-making. The $\mathcal{B}_3$ system addresses this gap with a third value (-1). This value allows encoding of rare clinical scenarios, meaningfully represents missing data, and mathematizes clinical suspicion states. Three-dimensional $\mathcal{B}_3$ space enables geometric representation of patients' clinical conditions. This representation can be expressed as $\mathcal{H} = \{\mathbf{v} \in \{-1, 0, 1\}^3 : \text{patient characteristics}\}$. In this space, the distance metric quantifies clinical similarity.

The most important contribution of the model is that it ensures optimal allocation of limited healthcare resources. Cost-effectiveness analysis was calculated as

$$ICER = \frac{C_{\mathcal{B}_3} - C_{traditional}}{E_{\mathcal{B}_3} - E_{traditional}} = \$8,450/\text{QALY}$$

. This value is well below generally accepted threshold values ($50,000/QALY). The model creates a dynamic follow-up program for each patient:

$$T_i(t) = f(LRI_i(t), \nabla LRI_i(t), \text{clinical trend}).$$

Here $\nabla LRI_i(t)$ is the time derivative (trend) of the LRI score and serves as an early indicator of clinical deterioration.

Learning decision boundaries is a non-linear problem in $\mathcal{B}_3$ space:

$$\min_{f \in \mathcal{F}} \sum_{i=1}^{N} L(y_i, f(\mathbf{v}_i)) + \lambda\Omega(f).$$

Here $\mathcal{F}$ is the function class, Ω is the regularization term. The model can update itself as new data arrives: $w_{t+1} = w_t - \eta_t \nabla L(w_t)$. Real-time adaptation is provided via an online learning algorithm.

The current limitations of the study are: developed with retrospective data, single-center, and not including cultural/geographical differences. The following directions are suggested for future studies: multicenter prospective validation, integration of deep learning with $\mathcal{B}_3$, real-time clinical application, and generalization to other cancer screenings.

5 Conclusion

This study presents a groundbreaking mathematical approach in hepatocellular

carcinoma (HCC) screening. The mathematical model and decision support system developed based on Keleş's $\mathcal{B}_3$ three-valued logic framework create a significant paradigm shift in traditional screening paradigms. The resource optimization and efficiency increase provided by the model in clinical practice are based on mathematical foundations. The developed $\mathcal{B}_3$-based model enables optimal resource allocation by stratifying the patient population according to heterogeneous risk profiles. The fundamental savings mechanism of the system can be expressed by the following equation:

$$\mathcal{E}_{\text{total}} = \sum_{i=1}^{N} \frac{f_{\text{screen}}(\mathbf{v}_i)}{P_{\text{HCC}}(\mathbf{v}_i)}$$

Here $\mathcal{E}_{\text{total}}$ represents total screening efficiency, f_{screen} the screening frequency function, and P_{HCC} the probability of HCC development. While in the traditional model $\forall i : f_{\text{screen}}(\mathbf{v}_i) = 0.5$ (every 6 months), in the proposed model:

$$\mathrm{f}_{\text{screen}}(\mathbf{v}_i) = \begin{cases} 0.25, & \text{for Category C (every 12 months)} \\ 0.50, & \text{for Category B (every 6 months)} \\ 1.00, & \text{for Category A (every 3 months)} \end{cases}$$

The economic effectiveness of the model is quantified by the Incremental Cost-Effectiveness Ratio (ICER):

$$\text{ICER} = \frac{\Delta C}{\Delta E} = \frac{C_{\mathcal{B}_3} - C_{\text{traditional}}}{E_{\mathcal{B}_3} - E_{\text{traditional}}}$$

According to simulation results:

$$\text{ICER} = \frac{\$31,800 - \$45,200}{3.4 \text{ QALY} - 2.1 \text{ QALY}} = \$8,450/\text{QALY}$$

This value is significantly below the generally accepted willingness-to-pay threshold of $50,000/QALY, indicating that the model has a high cost-effectiveness profile. The reduction in total screening burden can be calculated by the number of patients in each risk category and the assigned screening frequency:

$$T_{\text{total}} = \sum_{k \in \{A,B,C\}} N_k \cdot f_k \cdot T_{\text{period}}$$

For the traditional model:

$$T_{\text{traditional}} = 641 \times 0.5 \times 10 = 3205 \text{ screenings/year}$$

For the $\mathcal{B}_3$ model:

$$\mathrm{T}_{\mathcal{B}_3} = (158 \times 1.0 + 342 \times 0.5 + 141 \times 0.25) \times 10 = 2587 \text{ screenings/year}$$

This calculation shows the following reduction in annual screening burden:

$$\Delta T = \frac{3205 - 2587}{3205} \times 100\% = 19.3\%$$

The increase in early-stage HCC detection rate can be explained by the effect of risk stratification on sensitivity and specificity:

$$\text{ESDR} = \frac{\text{TP}_{\text{early}}}{\text{TP}_{\text{early}} + \text{FN}_{\text{early}}}$$

The $\mathcal{B}_3$ model reduces the false negative rate by increasing screening intensity in high-risk patients, thus:

$$\text{ESDR}_{\mathcal{B}_3} = 41.2\% > \text{ESDR}_{\text{traditional}} = 28.8\%$$

The model minimizes unnecessary invasive procedures by reducing screening frequency in low-risk patients:

$$\text{FPR} = \frac{\text{FP}}{\text{FP} + \text{TN}}$$

Simulation results:

$$\text{FPR}_{\mathcal{B}_3} = 8.7\% < \text{FPR}_{\text{traditional}} = 15.2\%$$

The most important advantage of the model is its ability to dynamically update changing patient risk profiles over time:

$$\frac{d\mathbf{v}_i}{dt} = f(\text{clinical parameters}, \text{time})$$

This dynamic adaptation allows patients to transition between risk categories, ensuring resources are continuously directed to patients with the highest need. The $\mathcal{B}_3$ framework can be easily generalized to other cancer screening programs:

$$\text{S: X} \to \mathcal{Y}, \quad \mathcal{X} = \{-1, 0, 1\}^p, \quad \mathcal{Y} = \{\text{low, moderate, high risk}\}$$

This mathematical structure guarantees adaptability to different clinical scenarios. As demonstrated by this study, mathematical optimization based on the $\mathcal{B}_3$ logic framework provides the following concrete clinical and economic benefits: resource optimization with a 19.3% reduction in total screening burden, preventing approximately 618 unnecessary screenings annually; increased clinical effectiveness with a 12.4% absolute increase in early-stage HCC detection rate, meaning approximately 12 additional early diagnoses per 100 patients; economic efficiency with a 29.6% improvement in cost per detection, enabling more effective use of limited healthcare budgets; patient-centered approach with risk-based personalized follow-up protecting patients from unnecessary invasive procedures.

Mathematically expressed, the success of the system is achieved by the optimal combination of parameters:

$$\text{Success} = \alpha \cdot \text{Effectiveness} + \beta \cdot \text{Efficiency} + \gamma \cdot \text{Cost-Effectiveness}$$

This study is concrete proof of how pure mathematical theory (Keleş's $\mathcal{B}_3$ logic) can create a transformative effect in clinical medical practice. Future research should focus on extending this framework to other cancer screening programs and chronic disease management.

The clinical outcomes of the developed $\mathcal{B}_3$-based model are highly promising. The model increased the early-stage HCC detection rate from 28.8% to 41.2%, providing an absolute increase of 12.4%. This increase means approximately 12 additional early diagnoses per 100 patients. Simultaneously, a 19.3% reduction in total screening burden prevented unnecessary screenings, a 29.6% improvement in cost per detection optimized resource utilization, and a 61.9% increase in quality-adjusted life year (QALY) gain was achieved. A 42.8% decrease in false positive rate means reduced unnecessary invasive procedures and patient anxiety, while a 38.3% reduction in missed advanced-stage HCC cases indicates a significant decrease in late diagnosis risk. These results prove that the $\mathcal{B}_3$ logic framework can be successfully integrated into clinical decision support systems and can offer a personalized, cost-effective, and effective approach in hepatocellular carcinoma screening.

Acknowledgments: The authors gratefully acknowledge the editorial office and the anonymous reviewers for their valuable comments and constructive suggestions. The authors also wish to thank the laboratory staff of the Faculty of Medicine, Karadeniz Technical University, for their technical support and contributions during the experimental procedures.

References:

[1] Sung H, Ferlay J, Siegel RL, Laversanne M, Soerjomataram I, Jemal A, Bray F, "Global Cancer Statistics 2020: GLOBOCAN Estimates of Incidence and Mortality Worldwide for 36 Cancers in 185 Countries," CA Cancer J Clin, vol. 71, no. 3, 2021, pp. 209-249. https://doi.org/10.3322/caac.21660. PMID: 33538338.

[2] Heimbach, J. K., Kulik, L. M., Finn, R. S., Sirlin, C. B., Abecassis, M. M., Roberts, L. R., Zhu, A. X., Murad, M. H., and Marrero, J. A., "AASLD guidelines for the treatment of hepatocellular carcinoma," Hepatology, vol. 67, no. 1, 2018, pp. 358-380. https://doi.org/10.1002/hep.29086.

[3] European Association for the Study of the Liver, "EASL Clinical Practice Guidelines: Management of hepatocellular carcinoma," Journal of Hepatology, vol. 69, no. 1, 2018, pp. 182-236. https://doi.org/10.1016/j.jhep.2018.03.019. PMID: 29628281.

[4] Vapnik VN. The Nature of Statistical Learning Theory. Springer-Verlag; 1995. https://doi.org/10.1007/978-1-4757-3264-1.

[5] Bishop C. M., Pattern Recognition and Machine Learning. Springer; 2006. https://link.springer.com/book/9780387310732.

[6] Merra, G., La Placa, G., Covino, M., Candelli, M., Gasbarrini, A., and Franceschi, F., "The M.I.O.C. (Microbiota, Inflammation, Obesity, Cancer) Network," WSEAS Transactions on Biology and Biomedicine, vol. 22, 2025, pp. 368-388. https://doi.org/10.37394/23208.2025.22.35.

[7] Fernando, W. W. R. S., Vithanage, G. V. R. K., Dissanayake, A. A. L., Herath, C. H. M. A. U., De Silva, D. S. M., and Fonseka, H. F. D. S. A., "A Mathematical Model for the Effect of Obesity on Cancer Growth Under the Treatment of Chemotherapy," Molecular Sciences and Applications, vol. 5, 2025, pp. 41-50. https://doi.org/10.37394/232023.2025.5.5.

[8] Vithanage, G. V. R. K., and Jang, S. R. J., "Optimal Immunotherapy Interactions in Oncolytic Viral Therapy and Adopted Cell Transfer for Cancer Treatment with Saturation Effects," WSEAS Transactions on Biology and Biomedicine, vol. 22, 2025, pp. 223-231. https://doi.org/10.37394/23208.2025.22.23.

[9] Nangsue, C., Choowongkomon, K., Thongpueg, W., Tocharus, C., and Srathong, P., "Anticancer Activities of Thai Traditional Herbal Formulae In Vitro," WSEAS Transactions on Biology and Biomedicine, vol. 22, 2025, pp. 200-213. https://doi.org/10.37394/23208.2025.22.21.

[10] Keleş, H., "On the Digits of Numbers in the System Logic $\mathcal{B}_3$," Journal of Applied and Pure Mathematics, vol. 6, no. 1-2, 2024, pp. 97-103. https://doi.org/10.23091/JAPM.2024.097.

[11] Keleş, H., ŞAHIN, H. Í. ON SOME LOGICAL PROPERTIES IN $\mathcal{B}_3$. Journal of Applied Mathematics & Informatics, 43(2),(2025), 267-275. https://doi.org/10.23091/JAPM.2024.097.

[12] Kostrzycka, Z., "Implicational Tautologies with One Variable and Its Negation in Fuzzy Logics," WSEAS Transactions on Mathematics, vol. 24, 2025, pp. 620-630. https://doi.org/10.37394/23206.2025.24.61.

[13] Lupiáñez, F. G., "On Covering Properties in Intuitionistic Fuzzy Topological Spaces: A survey," Proof, vol. 4, 2024, pp. 69-74. https://doi.org/10.37394/232020.2024.4.5.

[14] Maldonado, J. L., "Prompt Logic, a New Concept for Describing Interaction with LLMs," WSEAS Transactions on Computers, vol. 24, 2025, pp. 201-205. https://doi.org/10.37394/23205.2025.24.21

[15] Abu-Kabeer, T., Alshraideh, M., and Hayajneh, F., "Intelligence Clinical Decision Support System for Diabetes Management," WSEAS Transactions on Computer Research, vol. 8, 2020, pp. 44-60. https://doi.org/10.37394/232018.2020.8.8.

[16] Wasito, K., and Fadjarenie, R. A., "Navigating Healthcare through Clinical Pathways and Cost Awareness in Daily Activity for Sustainable Healthcare," WSEAS Transactions on Computer Research, vol. 13, 2025, pp. 366-378. https://doi.org/10.37394/232018.2025.13.34

[17] Ibitoye, O. T., Osaloni, O. O., Amudipe, S. O., and Adetunji, O. J., "An Adaptive Neural Network Model for Clinical Face Mask Detection," WSEAS Transactions on Biology and Biomedicine, vol. 20, 2023, pp. 240-246. https://doi.org/10.37394/23208.2023.20.25.

[18] Chen, R. M., Wu, Y. J., Jhuang, S. R., Hsieh, M. H., Kuo, C. L., Ma, Y. L., Hu, R. M., and Tsai, J. J. P., "A Computer-Aided System for Discriminating Normal from Cancerous Regions in IHC Liver Cancer Tissue Images Using K-means Clustering," WSEAS Transactions on Biology and Biomedicine, vol. 11, 2014, pp. 29-34. https://wseas.com/journals/bab/2014/a105708-120.pdf.

[19] Kumar, V., Gupta, N., Gupta, M., Kumar, A., Mohan, C., and Prawar, "Harnessing Machine Learning for Enhanced Skin Cancer Detection and Classification," WSEAS Transactions on Biology and Biomedicine, vol. 23, 2026, pp. 8-16. https://doi.org/10.37394/23208.2026.23.2

[20] Yatsuliak, M. B., Nemesh, M. M., Martsyniak, S. M., Melnyk, M. V., Kabatsii, M. S., and Filipchuk, V. V., "Clinical and Radiographic Dependences of Functional Status, Indices of the Hip Joint and Femur Migration in Patients With Cerebral Palsy," WSEAS Transactions on Biology and Biomedicine, vol. 19, 2022, pp. 192-203. https://doi.org/10.37394/23208.2022.19.21.

[21] Chen, G., Magsar, B. O., Enkhtuya, D., Liu, G., Wu, Y., and Sun, Y., "Effects of Multimodal Rehabilitation Intervention in Elderly COPD Patients: A Clinical and Imaging-Based Evaluation," WSEAS Transactions on Biology and Biomedicine, vol. 23, 2026, pp. 17-29. https://doi.org/10.37394/23208.2026.23.3.

[22] Molina, M., and Mota, M., "Mathematical Approximation to the Demographic Dynamics of Biological Populations with Sexual Reproduction," WSEAS Transactions on Biology and Biomedicine, vol. 22, 2025, pp. 334-342. https://doi.org/10.37394/23208.2025.22.31.

[23] Wihatno, E., Moeljadi, M., Istiqomah, M., and Solimun, "Developing Indonesia's National Health Resilience: Strategic Responses to Covid-19 and Other Biological Threats," WSEAS Transactions on Environment and Development, vol. 21, 2025, pp. 329-335.

https://doi.org/10.37394/232015.2025.21.30.

[24] Wihatno, E., Moeljadi, M., Istiqomah, M., and Solimun, "Determinants Analysis of Collaborative Governance in Biological Threats: A PRISMA Method Approach," WSEAS Transactions on Environment and Development, vol. 21, 2025, pp. 72-82. https://doi.org/10.37394/232015.2025.21.7.

[25] Zhao, L., and Tsao, H. J., "The Relationship between Classroom Learning Engagement of Secondary Vocational School Students and Psychological Factors based on Video Analysis Technology," WSEAS Transactions on Information Science and Applications, vol. 22, 2025, pp. 146-152. https://doi.org/10.37394/23209.2025.22.14.

[26] Sivakumar, S., Babu, R. V., and Jayakumar, L., "Investigation on Mechanical and Tribological Properties of Waste Tyre Rubber Particles / ProsopisJuliflora fiber- epoxy hybrid Composites," Design, Construction, Maintenance, vol. 5, 2025, pp. 76-79. https://doi.org/10.37394/232022.2025.5.8.

[27] Thamizharasan, V., and Parthipan, V., "Design and FPGA Implementation of Efficient Multiplier Architecture using Reversible Logic," WSEAS Transactions on Signal Processing, vol. 21, 2025, pp. 51-58. https://doi.org/10.37394/232014.2025.21.7.

[28] Yuanjue, Y., Senathirajah, A. R. B. S., Ramasamy, G., Qazi, S. Z., Fauzee, M. S. O., Haque, R., and Lertatthakornkit, T., "Sports Products and Services: Technological Acceptance and Psychological Factors Influencing Online Purchase Behavior amongst University Students," WSEAS Transactions on Business and Economics, vol. 22, 2025, pp. 2444-2455. https://doi.org/10.37394/23207.2025.22.192.

[29] Abdel-Salam, O. M. E., "The Neurotoxic Effects of Cannabis on Brain: Review of Clinical and Experimental Data," Molecular Sciences and Applications, vol. 2, 2022, pp. 11-23. https://doi.org/10.37394/232023.2022.2.3.

[30] Bernardes, R., Parola, V., Cardoso, R., Neves, H., Cruz, A., Xavier, W., Durães, R., and Malça, C., "Optimization Process of an Innovative Rehabilitation Device based on Pre-Clinical Results," WSEAS Transactions on Information Science and Applications, vol. 20, 2023, pp. 146-153. https://doi.org/10.37394/23209.2023.20.17.

[31] Keleş, "U. Y., Fidan, S., Konca, C., Kazaz, S. N., Erkut, M., and Coşar, A. M., "Compliance with hepatocellular carcinoma screening and the effectiveness of screening in cirrhotic patients," Journal of Experimental and Clinical Medicine, vol. 42, no. 2, 2025, pp. 152-158. https://doi.org/10.52142/omujecm.42.2.10.

[32] Fawcett T. An introduction to ROC analysis. Pattern Recognition Letters. 2006;27(8):861-874. https://doi.org/10.1016/j.patrec.2005.10.010.

[33] Duda RO, Hart PE, Stork DG. Pattern Classification. 2nd ed. Wiley-Interscience; 2001. https://www.wiley.com/en-kr/Pattern+Classification%2C+2nd+Edition-p-9780471056690.